Transport modeling of nonlinearly adsorbing solutes in physically heterogeneous pore networks

R. C. Acharya and S. E. A. T. M. Van der Zee

Soil Quality Section, Department of Environmental Sciences, Wageningen Universiteit en Researchcentrum, Wageningen, Netherlands

A. Leijnse

Department of Environmental Sciences, Wageningen Universiteit en Researchcentrum, Wageningen, Netherlands

[1]   The purpose of this study is to upscale nonlinearly reactive transport from the pore scale to a heterogeneous porous medium with the aid of a sufficiently large three-dimensional pore network model. We consider a porous medium that is chemically homogeneous (sorption reactivity is constant in space) but physically heterogeneous, as it has a spatially variable pore size. Our numerical experiments aim to assess whether traveling wave (TW) behavior develops and to assess how large a network is required to be to allow our conclusions. This study revealed that for this purpose the network should include more than a million pore units and that this size varies with the degree of heterogeneity. This assertion is based on temporal changes of the moments of a migrating front of nonlinearly adsorbing solute. In networks of equal sized pores, TW behavior occurs, and concentration distributions can be predicted by an analytical solution. For increasing physical heterogeneity the balance between the dispersive and adsorptive forces remains absent because the second central moment continues to grow as a function of time. The growth rate of this moment is a function of pore-scale heterogeneity.

Citation: Acharya, R. C., S. E. A. T. M. Van der Zee, and A. Leijnse (2005), Transport modeling of nonlinearly adsorbing solutes in physically heterogeneous pore networks, *Water Resour. Res.*, *41*, W02020, doi:10.1029/2004WR003500.

1.   Introduction

[2]   Both from the need to understand natural subsoil systems and because of contamination problems of soil and groundwater, the transport of solutes in porous media has become an important issue. The transport of solute is affected by the structure and texture of the porous medium. Additionally, solutes generally are not inert, but react among others with the porous medium. Such reactions may have a large impact on transport, and for this reason, much effort is being made to understand and quantify these effects. Because of the common limitations of scale and frequency of observations, experiments alone cannot provide this qualitative and quantitative understanding of transport, and mathematical modeling is needed [*Whitaker*, 1969; *Hassanizadeh and Gray*, 1979; *Celia et al.*, 1995].

[3]   Modeling is a scale-dependent process, which implies that the porous medium mass balance equations, such as the advection dispersion equation (ADE) contain effective coefficients [*Bear*, 1972]. Such coefficients require explicit upscaling [*Whitaker*, 1969; *Hassanizadeh and Gray*, 1979]. For porous media, upscaling starts at the pore scale, where pore-scale geometry and other properties affect both the macroscopic transport equations and their parameters. Pore network models may be regarded as elementary tools for upscaling [*Fatt*, 1956], because they enable us to develop understanding of the quantitative and qualitative effects of pore-scale heterogeneity [*Celia et al.*, 1995]. Because of their flexibility for upscaling, pore network models have already been applied for upscaling a number of phenomena [*Van Brakel*, 1975] such as multiphase flow dynamics [*Celia et al.*, 1995; *Hassanizadeh et al.*, 2002], porosimetry, hysteresis, diffusion, dispersion, and (relative) permeability [*Mohanty and Salter*, 1982; *Sahimi et al.*, 1986; *Dullien*, 1991; *Ioannidis and Chatzis*, 1993; *Tsakiroglou and Payatakes*, 2000; *Blunt et al.*, 2002; *Acharya et al.*, 2004b].

[4]   Using a simple pore network approach, it has been shown [*De Josselin de Jong*, 1958] that the ADE is valid for porous media. Analytical solutions have been provided for the ADE subject to different initial and boundary conditions, and for nonreactive and linearly adsorbing solutes [*Van Genuchten and Alves*, 1982; *Chrysikopoulos et al.*, 1990]. The combination of nonlinear adsorption and transport has received relatively little attention [*Serrano*, 2003]. Extending the ADE with a nonlinear reaction term, several studies showed that a traveling wave type of behavior may develop, which is characterized by a time invariant shape [*Bolt*, 1982; *Van der Zee*, 1990; *Van Duijn et al.*, 1993]. The combination of nonlinear sorption and transport in a 2-D pore network has been addressed [*Suchomel et al.*, 1998] for the case of biofilms. A 2-D network with a retardation factor
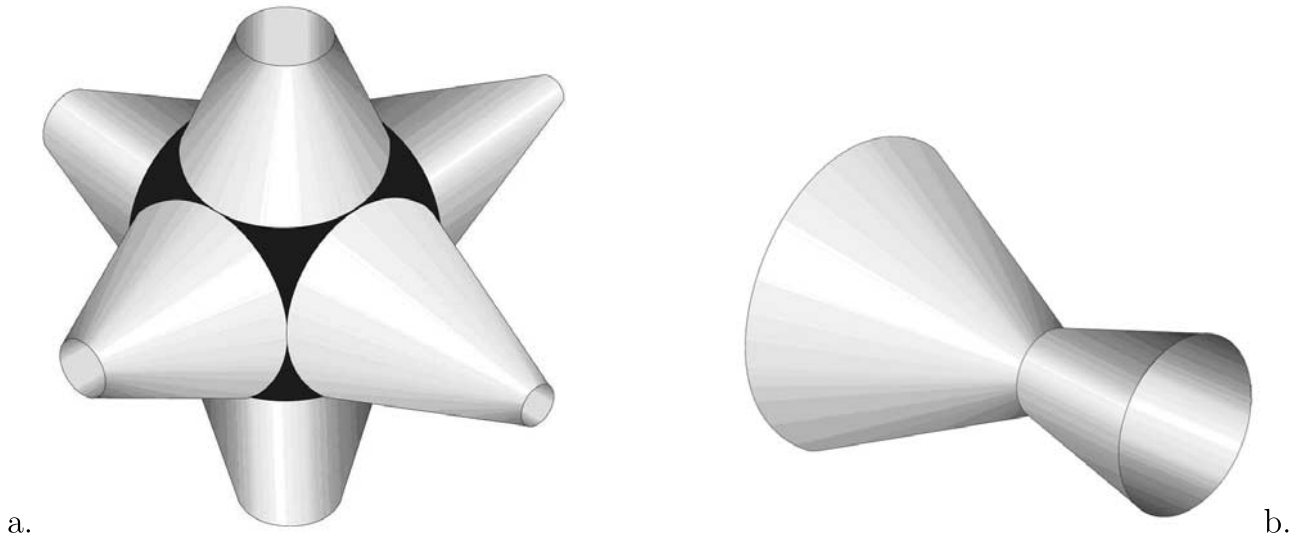
Figure 1. Basic elements of hydraulic pore network (HYPON): (a) pore unit (the pore body is marked with the dark shading) and (b) the biconical abscissa-asymmetric concentric (BACON) bond [*Acharya et al.*, 2004a].

that varies at the pore scale has also been considered [*Sugita and Gillham*, 1995]. To our best knowledge, the upscaling from 3-D pore networks to the continuum scale, where the ADE is valid, has never been done for the case of nonlinear sorption. Hence it is not justified that the extension of the ADE with a nonlinear adsorption term is appropriate.

[5] Important in upscaling is the ratio of the small process scale (ℓ) over the large system scale (or representative volume) (L), as the theory on volume averaging requires that $\ell \ll L$ [*Whitaker*, 1969; *Bear*, 1972; *Hassanizadeh and Gray*, 1979]. Only for proper scaling factors ($\tilde{\ell}$, where $\tilde{\ell} = \ell/L$), statistically stable and stationary effective parameters result. The appropriate scaling factor ($\tilde{\ell}$) depends on the type of process (or effective parameters) under consideration. For example, a 2-D pore network should comprise at least 35×35 nodes in order to produce an asymptotically effective hydraulic permeability (or conduc-

tivity) [*Koplik*, 1982], but a 3-D pore network can be as small as $25 \times 15 \times 15$ nodes [*Acharya et al.*, 2004a]. If a different process such as dispersion is considered, these size constraints may not apply [*Verlaan*, 2001]. Particle tracking studies that take diffusion (D_m) into account showed that a consistent value for the dispersion coefficient depends on the Peclet number ($v\ell/D_m$, with v, the average velocity across the network) [*Sahimi et al.*, 1986; *Acharya et al.*, 2004b]. Also at the capillary scale, Taylor-Aris theory suggests that the hydrodynamic dispersion depends on the aspect ratio and the capillary Peclet number [*Taylor*, 1953; *Aris*, 1956]. Hence the minimum scaling factor ($\tilde{\ell}$) and the minimal ergodic size of the pore network that is used for studying nonlinearly reactive transport need to be determined.

[6] The purpose of this paper is to apply a 3-D pore network model for upscaling nonlinear reactive transport
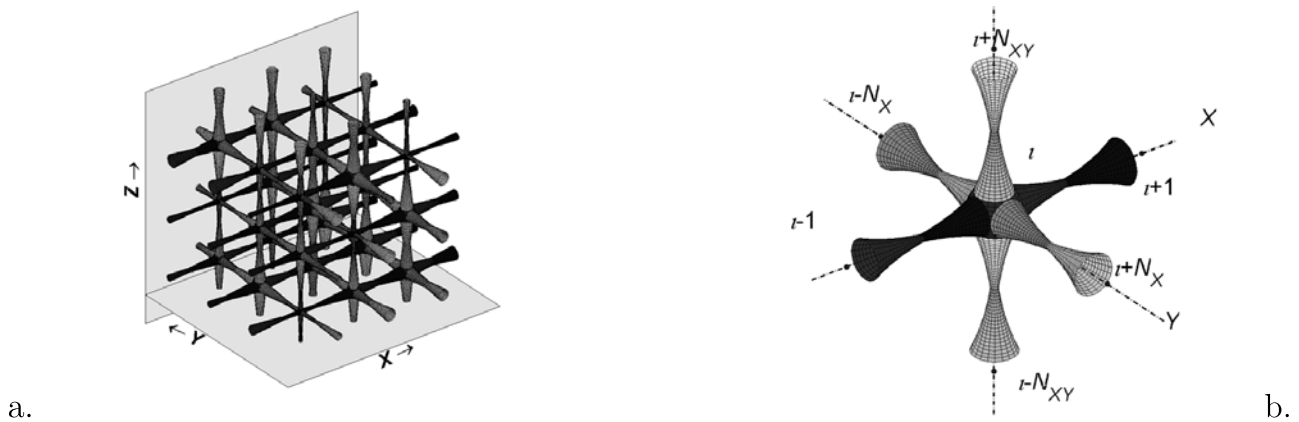

Figure 2. Three-dimensional pore network construction: (a) pore network as an aggregate of pore units and (b) typical connectivity scheme for a cubic lattice with pores of circular cross section shape [*Acharya et al.*, 2004a]. X, Y, and Z denote coordinate axes, N is the number of pore units as specified by the subscripts (N_X is along X, N_{XY} is in the XY plane), and ι is the index of the pore unit.

from the pore scale to a physically heterogeneous porous medium. Our numerical experiments are aimed at the assessment of whether traveling wave (TW) behavior develops because extending the ADE with a nonlinear adsorption term leads to such behavior for the used initial and boundary conditions. We also investigate the minimal ergodic size of the pore network.

2. Mathematical Formulation

[7] We consider two scales, which are the microscopic pore scale, and the macroscopic continuum scale (thousands of pores). Our pore network is a cubic lattice with a coordination number β equal to six, with pore units (PUs) as shown in Figure 1a as building stones. The centers of these pore units are placed at a regular grid length, i.e., the lattice constant ℓ and $\ell \ll L$. The symbol L denotes the length of the network. Each pore unit is composed of a pore body (large void) of radii R_{pb} (i.e., $R_{pb} = \widetilde{R}_{pb}\ell$ and $0 < \widetilde{R}_{pb} \leq 0.5$) and six converging cones (small voids) of different lengths (measured from the pore unit center). The cones from each two adjacent pore bodies form a converging-diverging biconical abscissa-asymmetric concentric bond (BACON bond), which varies along ℓ [Acharya et al., 2004a]. Depending on the wall curvature parameter (n), the BACON bonds are the union of two hyperbolic, parabolic or straight cones (Figure 1b) and the narrowest section is called the throat. For the construction of a pore network as shown in Figure 2 we refer to the original literature [Acharya et al., 2004a] and therefore do not repeat it here. In the following we introduce the equations of transport both in a pore and in a pore network.

2.1. Flow and Transport Equations at Pore Scale

[8] We assume that each elementary pore unit, as shown in Figure 1a, is perfectly mixed [De Josselin de Jong, 1958] and ignore molecular diffusion (D_m) by assuming that advection dominates the transport. Particle tracking simulations for pore networks showed that this assumption is valid for Peclet numbers ($Pe_\ell = v\ell/D_m$) between 10 and 10^4 [Acharya et al., 2004b]. For the mixing cell model (called hydraulic pore network (HYPON)), the transport equation for a PU is given by

$$V_{PU}\left(\frac{\partial c}{\partial t} + \frac{\partial s}{\partial t}\right) + \Sigma(\mathbf{q}c) = 0, \tag{1}$$

where V_{PU} (see notation section) is the fluid volume of the pore unit. We assume that sorption s (mass per fluid phase volume) is given by the Freundlich equation

$$s = kc^p, \tag{2}$$

where k is the adsorption coefficient and p is a parameter ($0 < p < 1$). Conventionally, s is expressed per mass of solid material, but as a pore has no solid mass, we have to define s differently. The symbol $\mathbf{q}$ denotes the discharge vector [$L^3 T^{-1}$] through bonds as shown in Figure 1b. For each bond connected to two nodes, discharge can be computed with Hagen-Poiseuille equation

$$q_{i,j} = \frac{g}{\nu}\ell^3 G_{i,j}(h_i - h_j), \tag{3}$$

where subscripts i and j are the addresses of nodes (fluid flows from i to j). $G_{i,j}$ denotes the dimensionless bond conductance derived earlier [Acharya et al., 2004a] in which both the longitudinal and cross sectional shapes of the bond are taken into account. Note that the geometric lengths are scaled by ℓ (pore spacing).

2.2. Transport Equations on Macroscopic Scale

[9] Assuming no-flow boundaries at the lateral sides of the pore network and introducing a head gradient in the longitudinal direction, a 1-D column is obtained. For such a column, the mass balance equation is given by the ADE,

$$\varepsilon\frac{\partial C}{\partial t} + (1 - \varepsilon)\rho_s\frac{\partial S}{\partial t} + \varepsilon v\frac{\partial C}{\partial X} = \varepsilon D_L\frac{\partial^2 C}{\partial X^2}, \tag{4}$$

where S is the adsorbed mass per unit mass of the solid phase [M M^{-1}], for example expressed in moles of adsorbate per kilogram of dry soil (with a density of ρ_s). Also at the macroscopic scale, we assume that adsorption the Freundlich equation,

$$S = K_F C^p, \tag{5}$$

where K_F is the adsorption coefficient and C is the concentration [M L^{-3}] expressed in terms of mass per unit volume of fluid. Combination of these two equations and dividing both sides of equation (4) by the porosity (ε), an average adsorption coefficient for the fluid phase can be defined as

$$\mu_k = K_F(1 - \varepsilon)\rho_s/\varepsilon. \tag{6}$$

For a chosen value of K_F, the average coefficient μ_k is computed on the basis of ρ_s and ε or vice versa. We assume that k of equation (2) equals μ_k and that k is the same in all pore units. Observe that for volumes smaller than the representative elementary volume (REV) [Bear, 1972], the porosity, density, and K_F are spatially variable. The dimensionless dispersivity (i.e., $\widetilde{\alpha}_L = \alpha_L/\ell$) can be estimated from the standard deviation ($\widetilde{\sigma}_{pb}$) of the dimensionless pore body radii ($\widetilde{R}_{pb} = R_{pb}/\ell$) according to Acharya [2004]

$$\widetilde{\alpha}_L\left(\langle\widetilde{R}_{pb}\rangle\right) = B_1\widetilde{\sigma}_{pb}^2 + B_2\widetilde{\sigma}_{pb} + \widetilde{\alpha}_0, \tag{7}$$

where the coefficients are constants, which are different for different ensemble average pore body radius ($\langle\widetilde{R}_{pb}\rangle$).

[10] It has been shown that the values estimated by this equations are in good agreement [Van der Zee et al., 2004] with those found with the more robust method of particle tracking [Acharya et al., 2004b]. In section 4 we show the results of both particle tracking and the mixing cell model for nonreactive solute transport.

[11] The macroscopic intrinsic (pore water) velocity v is determined with the Dupuit-Forcheimer equation

$$v = \frac{QL}{V_f}, \tag{8}$$

where Q is the macroscopic discharge across the pore network and V_f is its fluid volume [Acharya et al., 2004a].

[12] The initial and boundary conditions are given by

$$C(X > 0, t = 0) = C_{in}; \ C(0, t \geq 0) = C_0; \ \frac{\partial C}{\partial X}\bigg|_{(0,t>0)}$$
$$= 0; \ \frac{\partial C}{\partial X}\bigg|_{(L,t\geq 0)} = 0, \tag{9}$$

with $C_0 > C_{in}$.

2.3. Analytical Solutions

[13] In a homogeneous porous medium, equations (4) and (5) subject to the boundary and initial conditions equation (9) lead to traveling wave behavior if p is smaller than one and C_0 is larger than the initial one [*Van der Zee*, 1990; *Bosma and Van der Zee*, 1993]. Transforming according to

$$\eta = X - vt/R \tag{10}$$

the analytical solution for the traveling wave concentration distribution [*Van der Zee*, 1990; *Bosma and Van der Zee*, 1993], is

$$\widetilde{C}(\eta) = \begin{cases} \left\{ 1 - \exp\left[v(\eta - \eta^*)(1-p)(R-1)(RD_L)^{-1} \right] \right\}^m & \text{if } (\eta - \eta^*) \leq 0 \\ 0 & \text{otherwise,} \end{cases}$$

$$\tag{11}$$

where the dimensionless concentration is $\widetilde{C}(\eta) = (C(\eta) - C_{in})/(C_0 - C_{in})$, the parameter m equals to $1/(1 - p)$ and the retardation factor (R) is given by

$$R = 1 + \frac{\rho_s(1 - \varepsilon)}{\varepsilon} \frac{\Delta S(C)}{\Delta C}. \tag{12}$$

In equation (12), $\Delta C = C_0 - C_{in}$ and $\Delta S(C)$ is the corresponding change in the adsorbed mass. Further details are given in the original literature [*Van der Zee*, 1990; *Bosma and Van der Zee*, 1993]. If a nonreacting solute is considered, the solution is given by [*Van Genuchten and Alves*, 1982],

$$\widetilde{C}\left(\widetilde{X}, \widetilde{T}\right) = \frac{1}{2} \left\{ \text{erfc}\left[\frac{\widetilde{X} - \widetilde{T}}{2\sqrt{\widetilde{\alpha}_L \widetilde{\ell} \widetilde{T}}} \right] + \exp\left(\frac{\widetilde{X}}{\widetilde{\alpha}_L \widetilde{\ell}} \right) \text{erfc}\left[\frac{\widetilde{X} + \widetilde{T}}{2\sqrt{\widetilde{\alpha}_L \widetilde{\ell} \widetilde{T}}} \right] \right\}. \tag{13}$$

We assumed that $D_L \sim \alpha_L v$, and introduced $\widetilde{\ell} = \ell/L$, $\widetilde{X} = X/L$ and $\widetilde{T} = vt/L$. As $\widetilde{C}(X, t)$ can be interpreted as a probability function, the probability density function (PDF, $f(X)$) [*Bosma and Van der Zee*, 1993; *Keijzer et al.*, 2000] equals

$$f(X) = -\frac{\partial \widetilde{C}}{\partial X}. \tag{14}$$

2.4. Spatial Moments for Nonlinear Adsorption and Transport

[14] Since it has been shown that the validity of equation (11) can be evaluated more accurately with the second central spatial moment (M_2^c) than by comparing front shapes

of $C(X, t)$, we use the expression for M_2^c derived by *Bosma and Van der Zee* [1993]. We introduce

$$\widetilde{\eta} = (\eta - \eta^*) \leq 0, \ P = \frac{R - 1}{mR\alpha_L} \text{ with } m > 1, \chi_i = (-1)^i \frac{m!}{(m-i)!i!}, \tag{15}$$

for $i = 0, 1, 2, 3,\ldots m$ and m is an integer. With the first derivative of $\widetilde{C}(X, t)$ (i.e., equation (14)) spatial moments of all orders are computed:

$$M_n^c(t) = \frac{\int_{-\infty}^{\infty} [X - M_1(t)]^n f(X) dX}{\int_{-\infty}^{\infty} f(X) dX},$$

$$M_1(t) = \frac{\int_{-\infty}^{\infty} X f(X) dX}{\int_{-\infty}^{\infty} f(X) dX}, \ n = 2, 3, \ldots \tag{16}$$

$$\gamma = \frac{M_3^c}{\sqrt{\left(M_2^c\right)^3}}, \qquad \kappa = \frac{M_4^c}{\left(M_2^c\right)^2}, \tag{17}$$

where subscript n denotes the order of spatial moments and the superscript c indicates "central", e.g., $M_1(t)$ is the first spatial moment at time t. Symbol γ denotes the coefficient of skewness or the measure of symmetry, whereas κ is the coefficient of kurtosis. For a normal distribution $\gamma = 0$ and $\kappa = 3.0$. A skewed distribution possesses γ other than zero. The distribution with $\kappa > 3$ is leptokurtic, for κ less than three it is platykurtic. For the case of nonreactive tracer transport, the dispersivity can be expressed in terms of the Einstein's relation [*Chandrasekhar*, 1943], i.e.,

$$\alpha_L = 0.5 \frac{M_2^c(t_2) - M_2^c(t_1)}{M_1(t_2) - M_1(t_1)}, \tag{18}$$

where t_1 and t_2 are the times. For a TW, the second central moment (M_2^c), i.e., the spatial variance of the front asymptotically approaches a fixed value which is given by

$$M_2^c = -\frac{1}{P^2} \left[2\sum_{i=1}^{m} \frac{\chi_i}{i^2} + \left(\sum_{i=1}^{m} \frac{\chi_i}{i} \right)^2 \right], \ i \geq 1 \tag{19}$$

and the higher-order spatial moments also approach a fixed value [*Bosma and Van der Zee*, 1993; *Keijzer et al.*, 2000].

3. Numerical Procedure

[15] Imposing a hydraulic head difference across the pore network in the X direction, system of equations for steady state flow is solved for hydraulic heads and subsequently the discharges through the bonds (equation (3)) are calculated. The computation of transport in pore units, equation (1) depends on these discharges. At the macro-

Table 1. Microscopic and Macroscopic Input Parameters for the Numerical Experiments[a]

	Case				
	S000	S030	S060	S086	S115
min $\widetilde{R}_{pb}$	0.300	0.248	0.204	0.152	0.100
max $\widetilde{R}_{pb}$	0.300	0.352	0.412	0.450	0.500
$\widetilde{\sigma}_{pb}$	0.000	0.030	0.060	0.086	0.115
ε	0.240	0.243	0.265	0.267	0.285
μ_k	8.11	7.96	7.09	6.88	6.39
R	9.11	8.96	8.09	7.88	7.39
$\widetilde{\alpha}_L$	0.434	0.496	0.614	0.764	0.982
Pe_ℓ	384	386	430	405	420

[a]Coefficient μ_k is computed based on fixed K_F, the density of the solid phase (ρ_s), and the porosity (ε) of modeled porous medium. Here $\widetilde{\alpha}_L|_{\langle\widetilde{R}_{pb}\rangle=0.30} = 32.11\widetilde{\sigma}_{pb}^2 + 1.072\widetilde{\sigma}_{pb} + 0.4344$ (see equation (7)).

scopic scale, we use the analytical solution (equation (11)) to predict the concentration profiles along the mean flow direction, because v, D_L and R are known [*Bosma and Van der Zee*, 1992].

3.1. Numerical Scheme for Microscopic Approximation

[16] Under initial and boundary conditions given by equation (9) the numerical scheme for the computation of transport in a pore unit can be written as

$$
c(i, t+\Delta t) - c(i, t) + k[c(i, t+\Delta t)]^p - k[c(i, t)]^p
$$
$$
= \underbrace{\frac{\Delta t}{V_{PU}}\left(\sum_j c(j, t)q_{j,i} - c(i, t)(q_{PU})_i\right)}_{\Delta c(i,t)_{AD}},
$$
(20)

where the index j is chosen such that $h_j > h_i$. The node discharge $(q_{PU})_i$ is the sum of the flows entering or leaving the node i, i.e.,

$$
(q_{PU})_i = \sum_j |q_{j,i}|, \qquad h_j > h_i, \qquad j = 1, 2, 3 \ldots \beta. \quad (21)
$$

Rewriting equation (20) as

$$
c(i, t+\Delta t) + k[c(i, t+\Delta t)]^p = \Delta c(i, t)_{AD} + k[c(i, t)]^p
$$
$$
+ c(i, t) = B(i, t+\Delta t), \quad (22)
$$

the resulting equation (22) can be solved using an optimization technique, such as Newton-Raphson [*Sun*, 1996]. For the stability of the scheme, the minimum time step is chosen on the basis of pore unit residence times,

$$
2\Delta t \le \min\{[\mathbf{V}_{PU}][\mathbf{q}_{PU}^{-1}]\} = \min\{\mathbf{T}_{PU}\} \quad (23)
$$

In equation (23), $\mathbf{V}_{PU}$ and $\mathbf{q}_{PU}$ are the matrix vectors of pore unit volumes and total (absolute) discharges from (or into) the pore units [*Acharya et al.*, 2004a] respectively, and $\mathbf{T}_{PU}$ is the matrix vector of pore unit residence times. Average concentration for each pore unit is updated at the end of each Δt. The average

concentration for each pore unit is updated after each time step.

3.2. Numerical Scheme for Macroscopic Approximation: Averaging

[17] At designated time steps ($\gg\Delta t$), the concentrations of pore units of the same X coordinate of the pore network are averaged. To avoid boundary effects, we consider the pore units of the inner core only by excluding a volume at each no-flow boundary of 5ℓ thickness. For averaging, the discharges out of the PU (or into the PU) are used as the weighting factors of the corresponding PU concentrations. Hence the resulting dimensionless concentration function $\widetilde{C}(X, t)$ for a 1-D column (at the network scale) is given by

$$
\widetilde{C}(X, t) = \left[\frac{\sum_i^{N_t} c(i, t)(|q_{PU}|)_i}{\sum_i^{N_t} (|q_{PU}|)_i} - C_{in}\right]\frac{1}{C_0 - C_{in}}, \quad i = 1, 2, 3 \ldots N_t,
$$
(24)

where the symbol N_t denotes the total number of pore units that are indexed with i and that possess the same coordinate X. The X coordinate is chosen at an interval of ℓ, i.e., $X = 0$, 1ℓ, 2ℓ, ... L. The PDF (14) is discretized by choosing $\partial X \approx \ell$, i.e

$$
f\left(X + \frac{1}{2}\ell, t\right) = -\frac{\widetilde{C}(X+\ell, t) - \widetilde{C}(X, t)}{\ell}. \quad (25)
$$

4. Simulation Cases

[18] As no recommendation for the pore network size can be found in the literature, for the case of nonlinear adsorption, a trial and error approach was followed. Preliminary simulations suggested that at least a million (10^6) pore units are required to achieve the asymptotic growth rates of second central moments of nonlinearly adsorbing solute migration in a microscopically heterogeneous medium. Hence we use a cubic pore network of size $301 \times 61 \times 61$ pores for the reported simulations. To capture effects of microscopic heterogeneity on transport, five systematic cases (S000, S030, S060, S086 and S115) that are listed in Table 1 were considered. The pore units are constructed with the curvature parameter (n) equal to one and the ensemble of dimensionless pore body radii ($\widetilde{R}_{pb}$, with $\widetilde{R}_{pb} = R_{pb}/\ell$) taken from a uniform distribution [*Acharya et al.*, 2004a].

[19] Table 1 identifies case S000 as a homogeneous medium, whereas the other cases represent physically heterogeneous media. In all cases, we fixed the mean ($\langle\widetilde{R}_{pb}\rangle$) of the pore body radii at 0.30, and for each case we generated a pore network with a chosen standard deviation ($\widetilde{\sigma}_{pb}$) of $\widetilde{R}_{pb}$ that varies from zero (case S000) to 0.115 (case S115). In all cases the macroscopic hydraulic head drop across the network was fixed at 0.07 m. Additionally, $\ell = 0.25 \times 10^{-3}$ m and $D_m = 8.0 \times 10^{-10}$ m^2/s (*Taylor*'s [1953] data) are used for the Brownian particle tracking model [*Acharya et al.*, 2004b]).

[20] As Table 1 shows, the cases have different average porosities (ε). Consequently, although we choose the same
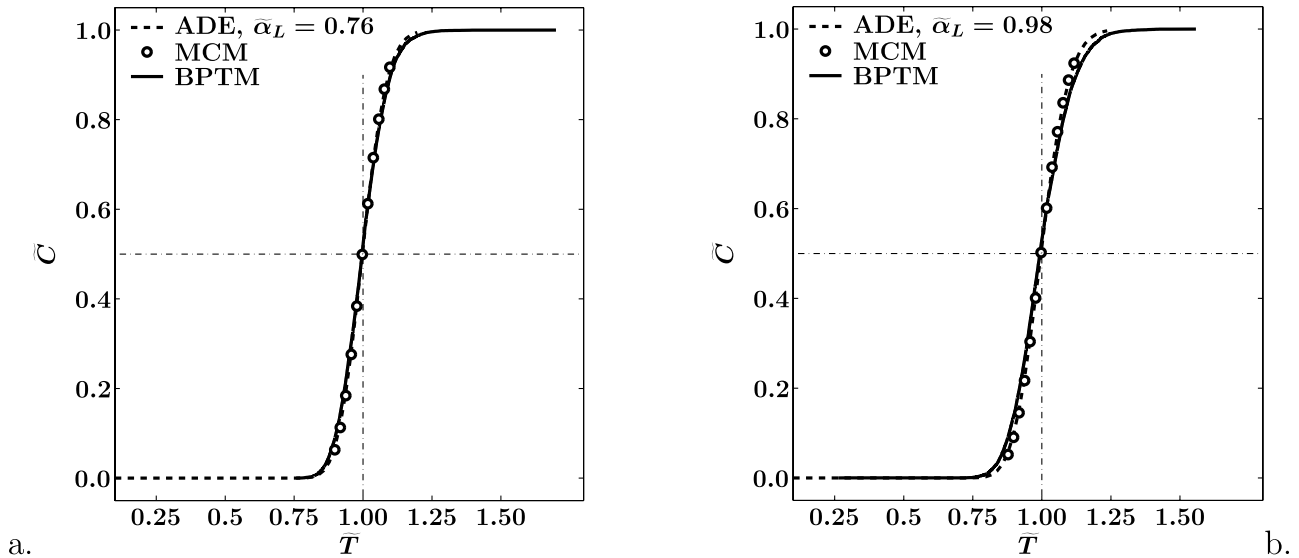
Figure 3. Breakthrough curves at the outlet face of the network. (a) Case S086. (b) Case S115. MCM (open circles) indicates the results of numerical simulations from pore network model HYPON (equation (24)), BPTM (solid lines) indicates the results from the simplified network in which Brownian particle-tracking procedure is applied [*Acharya et al.*, 2004b], and CDE (dashed lines) indicates the results from equation (13) with $\widetilde{\alpha}_L$ of Table 1 (and as displayed here).

influent of unit concentration ($C_0 = 1$ g/m^3) for injection and same value of K_F, the average value of μ_k (and also k) differs from case to case. The cause of such differences follows from equation (6), that shows the dependency on the density and porosity of the porous medium. The values of μ_k are calculated on the basis of $\rho_s = 2.6$ Mg/m^3, $K_F = 0.982 \times 10^{-3}$ (Mg/Mg)/(1 g/m^3)^p and the average porosity (ε). The parameter p is fixed at 0.667 and $C_{in} = 0$. We assume k to be constant within each whole network, i.e., k in each pore unit is constant in space and time. The retardation factor R is calculated with equation (12).

[21]   In Table 1, $\widetilde{\alpha}_L$ was calculated with equation (7) and a comparison was made for cases S086 and S115 for a nonreactive tracer ($K_F = 0$), with the mixing cell model (MCM) and the Brownian particle tracking model (BPTM) [*Acharya et al.*, 2004b]. The breakthrough curves at the outlet face of the networks for both methods are shown in Figure 3. Also the BTC computed with equation (13) by using $\widetilde{\alpha}_L$ is shown. The differences can be attributing to disregarding molecular diffusion in HYPON. The differences indicate that the effect of molecular diffusion is minor. Figure 3 reveals that the BTC from BPTM is more dispersed than the one from HYPON, which is theoretically correct. Differences are larger for case S115 than for case S086, which may be due to the effect of large aspect ratios (bond radius to ℓ ratio), where particle tracking models are quite
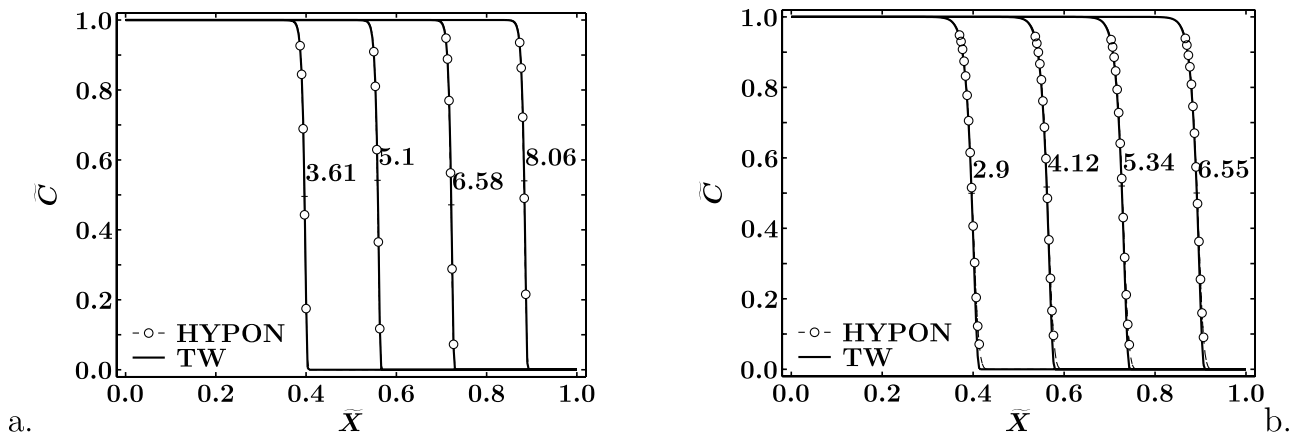

Figure 4. Dimensionless concentration profiles at different times as a function of fraction of column length ($\widetilde{X} = X/L$) (a) Case S000. (b) Case S115. HYPON (dashed lines with open circles) indicates the results of numerical simulations from pore network model HYPON (equation (24)), and TW (solid lines) indicates the analytical TW solution (equation (11)) with the same adsorption coefficient (see also Table 1). The labels of curves indicate the times, i.e., the pore volumes of effluent discharged from the network.
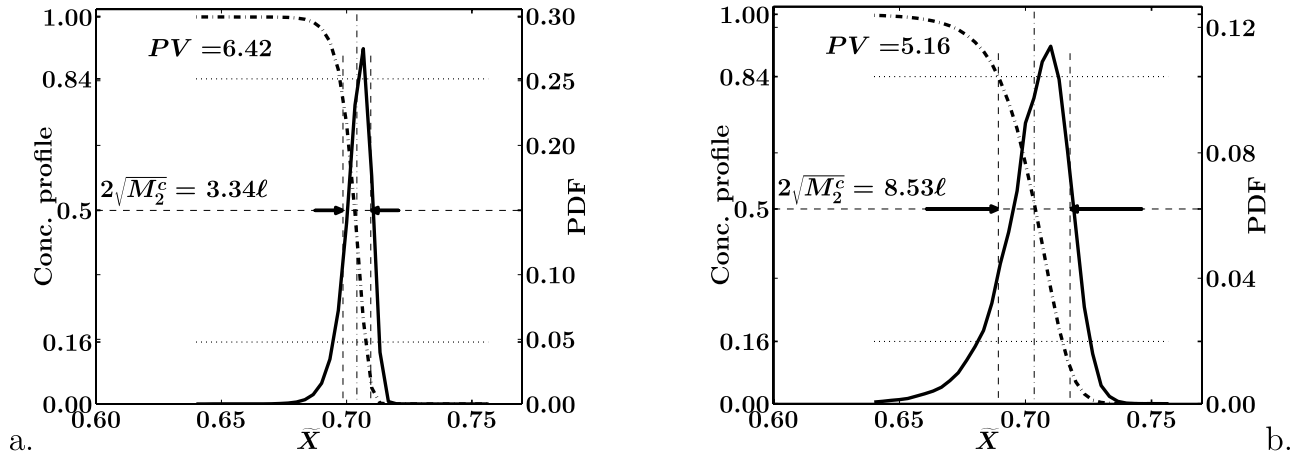
Figure 5. Typical PDFs ($f(X)\ell$) of concentration profiles in a pore network. (a) Case S000. (b) Case S115. Shown are the PDFs (solid lines) and concentration profile (dash-dotted lines) at the chosen times (PV) as shown here, i.e., number of pore volumes (PV) discharged from the network. The values of $2\sqrt{M_2^c}$ at times $\widetilde{T} = PV$ are shown.

sensitive [*Sorbie and Clifford*, 1991]. Since we expect that the nonlinearity of adsorption decreases the diffusion within individual pores (see section 2.4), the results obtained with HYPON are expected to be valid, and the values of $\widetilde{\alpha}_L$ given in Table 1 are reasonable approximations.

[22] We considered case S086* (a separate realization with the same statistics as of S086) for the consistency test, with the aim to assess whether the used network size is ergodic. A second case S086** was used for verifying the moment growth rate and pore radii statistics relations. For this case, the varied parameters are $\langle \widetilde{R}_{pb} \rangle = 0.25$, $\widetilde{\sigma}_{pb} = 0.086$, $\varepsilon = 0.194$ and $\mu_k = 10.57$ (g/m^3)$^{1-p}$.

5. Results

[23] The primary results of the numerical simulations are the nonlinear concentration profiles at different times (see equation (24)). These profiles form the basis of the moment analysis.

5.1. Concentration Profiles

[24] In Figure 4a the dimensionless (numerical) concentration profiles for case S000 are shown. On the macroscopic scale the TW solution (i.e., equation (11)) is used with upscaled adsorption coefficient (equation (6)) to predict the concentration profiles analytically and is also shown in Figure 4a. Figure 4 shows that numerical and analytical profiles are almost indistinguishable. The agreement indicates that for a microscopically homogeneous medium traveling wave behavior occurs at the macroscopic scale and the front shape and velocity become constant as a function of time. A similar comparison is shown in Figure 4b for case S115, which case represents a microscopically heterogeneous medium. Unlike in the previous case, differences are found, particularly at low concentrations.

5.2. Second Central Moment

[25] For additional comparison of the analytical and numerical results, spatial moments are calculated. Figure 5a gives an impression of the PDF produced by case S000 and Figure 5b shows the PDF of case S115. We observe that for these two cases the behavior of the fronts of

the tracer profiles is not the same as the front is more dispersed for case S115. In both cases, PDFs are skewed which indicates non-Fickian behavior. In Figure 6, the second central moments for all cases are shown as a function of the first spatial moment.

[26] Figure 6 reveals that for case S000 convergence occurs to the TW because after some transition length M_2^c, acquires an asymptotic value [*Van der Zee*, 1990; *Bosma and Van der Zee*, 1993]. For the other cases, we observe no asymptotic behavior, as the slopes of the fitted lines ($\widehat{M}_2^c$) are larger than zero and increase with increasing heterogeneity (see Table 1). At time $t = t_{tr}$, the second central moment reaches a value b, which also increases as heterogeneity increases. The fitted lines follow the regression equation for $\widehat{M}_2^c$ given by

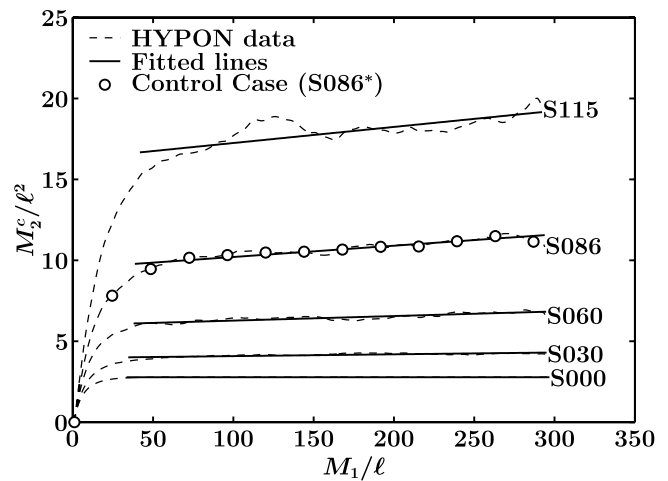$$\widehat{M}_2^c(t) = \alpha_{res}[M_1(t) - M_1(t_{tr})] + b, \ t > t_{tr}, \qquad (26)$$

Figure 6. Dimensionless second central moments (M_2^c/ℓ^2) and fitted lines. Second central moments (dashed lines) are as a function of M_1/ℓ, and the fitted lines (solid lines, $\widehat{M}_2^c/\ell^2$, equation (26)) are for cases as identified at the lines. M_2^c of the control case S086* are indicated as circles.

Table 2. Parameters of Linear Equation Fitting to the Numerical Second Central Moments[a]

	Case				
	S000	S030	S060	S086	S115
α_{res}/ℓ	0.0000	0.0011	0.0028	0.0070	0.0099
b/ℓ^2	2.7760	4.0046	6.0957	9.7764	16.6647
r^2	0.9999	0.7739	0.9021	0.9312	0.7695

[a]See Figure 6.

where α_{res} is the slope which is valid after a transition time (t_{tr}). In analogy with equation (18), $\frac{1}{2}\alpha_{res}$ can be seen as the reduced dispersivity of nonlinearly adsorbing transport. Both α_{res} and b are presented in Table 2. The coefficients of correlation (r^2) of M_2^c and $\widehat{M}_2^c$ are also given in Table 2.

[27] Figure 6 shows that the goodness of fit for the regression analysis differs. Case S000 shows a perfect agreement with the numerical data. Cases S030 and S060 also show a good agreement. In case S086 individual deviations are noticeable. However, the statistical stability of the used network size cannot be questioned, because the control case (S086*) closely aligns with the base case (S086). This agreement affirms the sufficiency and ergodicity of the pore network of size $301 \times 61 \times 61$ (at least for the chosen data set) and that Monte Carlo simulations are not necessary to reach robust conclusions. Unfortunately, in case S115, the deviations are the largest (with smallest r^2 in Table 2), which indicates that the chosen network might still be too small to accommodate the chosen pore size statistics of this case. In view of the computational demand, a network larger than the size $301 \times 61 \times 61$ could not be simulated. Hence it may be expected that the precise value of the fitted constants may deviate from those in Table 2 for this case. In Figure 7a the slopes (α_{res}) and intercepts (b) of $\widehat{M}_2^c$ (see Table 2) are shown as a function of the standard deviation of pore body radii (see Table 1). To verify the validity of the fitted equations for other ensemble averages ($\langle \tilde{R}_{pb} \rangle$), the values of α_{res} and b of case S086** are also

shown but with different symbols (see figure). The data are fitted with quadratic equations of the standard deviation of pore body radii given by

$$\widehat{\alpha}_{res} = \left(0.588\widetilde{\sigma}_{pb}^2 + 0.0212\widetilde{\sigma}_{pb}\right)\ell \quad (27)$$

$$\widehat{b} = \left(1057.3\widetilde{\sigma}_{pb}^2 - 4.8965\widetilde{\sigma}_{pb} + 2.7760\right)\ell^2, \quad (28)$$

These relations thus functionally link the heterogeneity in the pore size and the degree of front spreading. Note that these relations are valid for a particular mean pore body radii ($\langle \tilde{R}_{pb} \rangle = 0.30$), which can also be seen with the deviation of α_{res} of case 086**. Alternatively, these parameters can be fitted with respect to the coefficient of variation of the pore body radii:

$$\widehat{\alpha}_{res} = \left(0.532\eta_{pb}^2 + 0.0063\eta_{pb}\right)\ell \quad (29)$$

$$\widehat{b} = \left(11.66\eta_{pb}^2 + 1.67\eta_{pb} + \sqrt{2.776}\right)^2\ell^2. \quad (30)$$

[28] In Figure 7b, α_{res} and b are shown as a function of η_{pb} together with the fitted functions. Figure 7b shows that the agreement of the fitted functions with the data is better for the intercept than for the slope. Figure 7b reveals that the values of case S086** do not fall on the regression line. Apparently, if the mean pore size is changed, whereas the pore size variability is kept constant, still a new set of simulations is needed. Looking at the difference between S086** and S086 in Figure 7a we see that the marker for b falls close to the fitting line, which may suggest that during the transition phase, absolute variability controls spreading instead of relative variability.

5.3. First- and Higher-Order Spatial Moments

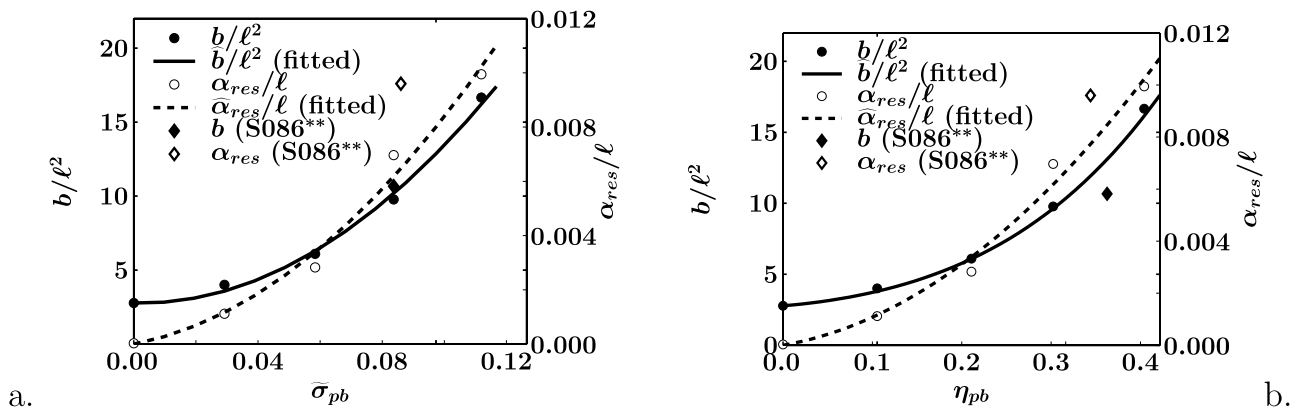[29] The higher-order spatial central moments are the quantitative measure of width (M_2^c), symmetry (γ) and

Figure 7. Slopes and intercepts. (a) Slopes (α_{res}) and intercepts (b) of $\widehat{M}_2^c$ as a function of standard deviation ($\widetilde{\sigma}_{pb}$) of pore body radii. The solid line (fitted, $\widehat{b}$) and the solid circles (b) indicate intercepts; the dashed line (fitted, $\widehat{\alpha}_{res}$) and the open circles (α_{res}) indicate the slopes (see Table 2 and equations (27) and (28)). (b) Slopes (α_{res}) and intercepts (b) of $\widehat{M}_2^c$ as a function of coefficient of variation of pore body radii ($\eta_{pb} = \widetilde{\sigma}_{pb}/\langle \tilde{R}_{pb} \rangle$). The solid line (fitted, $\widehat{b}$) and the solid circles (b) indicate intercepts; the dashed line (fitted, $\widehat{\alpha}_{res}$) and the open circles (α_{res}) indicate the slopes. The solid diamond indicates the intercept, and the open diamond indicates the slope α_{res} of the verifying case S086** (see Table 2 and equations (27) and (28)).
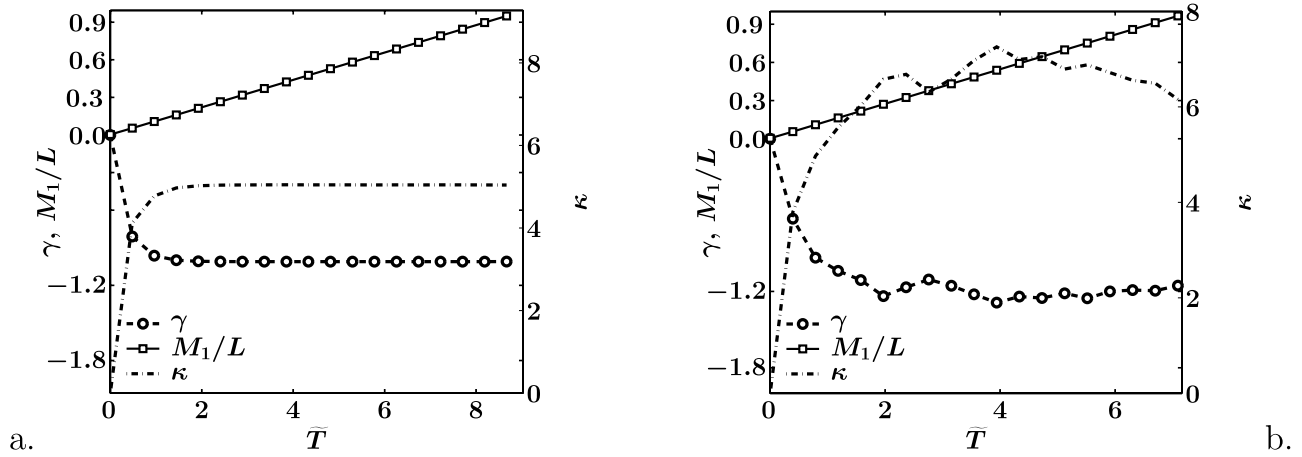
Figure 8. Macroscopic spatial first moment, skewness (γ), and kurtosis (κ) of plume (Table 1) as a function of pore volume of the effluent. (a) Case S000. (b) Case S115. The legends are shown.

peakedness (κ) of the concentration distribution function, and the first spatial moment shows the location of front. In Figure 8 these spatial moments, are shown for case S000 and S115.

[30] Figure 8 is direct evidence of non-Fickian transport for both cases, although the nature of this non-Fickian behavior differs. We observe that the growth of M_1 is constant as a function of time, which is necessary as the transport velocity is based directly on the mass balance (the injection rate of solute is constant). After a transition time t_{tr}, both skewness (γ) and kurtosis (κ) become asymptotic and stable for S000. The value of γ indicates that the wave shape is skewed negatively, and non-Gaussian (as for Fickian transport $\gamma = 0$). The kurtosis differs also from the value (three) of the normal distribution function. Although similar observations can be made for case S115 (see Figure 8a), namely, that we deal with non-Fickian transport. Different from case S000, transport does also deviate from traveling wave behavior (in view of the second central moment). For this case, the skewness and kurtosis do not stabilize as a function of time. The limited stability of higher-order moments is known to be an indication of the need to increase the domain size. However, at this stage it is not possible to evaluate whether this instability is singularly caused by the restricted size of the pore network, as the larger pore networks are costly with respect to the simulation times and the memory requirements. For example, the CPU time for case S115 is 147 CPU hours on a Pentium 4 (2.6 GHz) machine with a RAM of 1 GB. Whereas neither case S000 nor case S115 can be described with Fickian type solutions such as

$$\widetilde{C} = \frac{1}{2}\mathrm{erfc}\left[\frac{X - vt}{2\sqrt{D_L t}}\right], \tag{31}$$

for case S000 we still have the traveling wave solution available. For case S115, no analytical solution is known, to our best knowledge.

6. Conclusions

[31] We modeled five cases of a macroscopically homogeneous and isotropic medium with the aid of a pore network. Each of these cases was constructed with different variances of pore body radii but the same mean size. Hence we considered pore networks ranging from microscopically homogeneous ($\widetilde{\sigma}_{pb} = 0$) to microscopically heterogeneous ($\widetilde{\sigma}_{pb} > 0$). A trial and error approach was used to determine an ergodic size of the 3-D pore network. For the discussed simulations, a size of $301 \times 61 \times 61$ nodes was accepted as a minimum size and was evaluated by comparing two different realizations of one of the networks. We expect that the minimum network size depends on pore body variability, hydraulic and chemical parameters. To systematically assess these dependencies is numerically quite demanding.

[32] In this paper, we established that nonlinearity of adsorption (and possibly of other types of nonlinear reactions) at the microscopic scale has a large effect on the macroscopic transport behavior. Whereas for a physically homogeneous case, transport shows a traveling wave behavior, this is not the case for a case that is at the pore scale physically heterogeneous. Neither the homogeneous nor the heterogeneous cases show Fickian transport at the macroscopic scale. This implies for the microscopically heterogeneous case, analytical solutions as reported in the literature that we are aware of, are lacking. Our observations also raise questions regarding the validity of the transport equation at the macroscopic scale. If the heterogeneous case deviates from traveling wave behavior then it may be inappropriate to extend the ADE with a nonlinear reaction term, as for the considered initial and boundary conditions such an extended equation leads to a traveling wave.

Notation

c, C microscopic and macroscopic concentration [M L^{-3}].

Δc_{AD} microscopic concentration increment [M L^{-3}].

C_0, C_{in} influent and initial effluent concentrations [M L^{-3}].

D_m, D_L molecular diffusion and longitudinal dispersion coefficients [L^2 T^{-1}].

$G_{i,j}$ dimensionless conductance.

h_i, h_j hydraulic heads [L].

k microscopic sorption coefficient $[(\text{M L}^{-3})/(\text{M L}^{-3})^p]$.

K_F macroscopic sorption coefficient $[(\text{M M}^{-1})/(\text{M L}^{-3})^p]$.

ℓ, L node-to-node (bond) and the network lengths [L].

$\widetilde{\ell}$ scaling factor (ℓ/L) (dimensionless).

M_1, M_n first [L] and nth spatial moments $[\text{L}^n]$.

$M_2^c, b, \widehat{b}$ second central moment, $\widehat{b} = M_2^c$ $(t = t_{tr})$ and $b \sim \widehat{b}$ $[\text{L}^2]$.

N_t total number of pore units included in the inner core of the chosen tier.

N_X, N_{XY} number of nodes along X and XY planes.

Pe_ℓ, α_L characteristic Peclet number ($v\ell/D_m$) and dispersivity (D_L/v) (dimensionless).

$\mathbf{q}, q_{i,j}, Q$ discharges: vector, through bond i, j and through pore network $[\text{L}^3 \text{ T}^{-1}]$.

R retardation factor (dimensionless).

$R_{pb}, \widetilde{R}_{pb}$ dimensionfull [L] and dimensionless pore body radius ($\widetilde{R}_{pb} = R_{pb}/\ell$).

s microscopic sorption, mass absorbed per unit volume of fluid $[\text{M L}^{-3}]$.

S macroscopic sorption (mass of solute absorbed/mass of solid phase) $[\text{M M}^{-1}]$.

$t, t_{tr}, \Delta t$ time, transition time, and time step of iteration [T].

$\mathbf{T}$ residence time vector [T].

v mean intrinsic velocity along the principle flow direction in the pore network $[\text{L T}^{-1}]$.

V_{PU}, V_f pore unit and total fluid phase volumes $[\text{L}^3]$.

x, X local (along bond $0 \leq x \leq \ell$) and global (along network $0 \leq X \leq L$) axis.

$\alpha_{res}, \widehat{\alpha}_{res}$ M_2^c growth rates with respect to M_1 after transition times [L].

γ coefficient of skewness (dimensionless).

κ coefficient of kurtosis (dimensionless).

ε porosity (dimensionless)

μ_k mean adsorption coefficient

ν coefficient of kinematic viscosity $[\text{L}^2 \text{ T}^{-1}]$.

$\widetilde{\sigma}_{pb}^2$ variance of dimensionless pore body radii $\widetilde{R}_{pb}$.

Subscripts

(i,j) indices of nodes.

L longitudinal.

m molecular.

pb pore body.

PU pore unit.

n nth.

tr transition.

t tier.

Superscripts

c central.

Angle brackets indicate ensemble average.

References

Acharya, R. C. (2004), Upscaling of nonlinear reactive transport: From pore to core, Ph.D. thesis, 137 pp., Wageningen Univ., Wageningen, Netherlands.

Acharya, R. C., S. E. A. T. M. Van der Zee, and A. Leijnse (2004a), Porosity-permeability properties generated with a new 2-parameter 3D hydraulic pore network model for consolidated and unconsolidated porous media, *Adv. Water Res.*, 27(7), 707–723.

Acharya, R. C., M. I. J. Van Dijke, A. Leijnse, S. E. A. T. M. Van der Zee, and K. S. Sorbie (2004b), Upscaling of tracer transport including convection and Brownian motion using a 3D network model, in *Proceedings of Computational Methods in Water Resources June, 2004, Chapel Hill, NC*, vol. 1, edited by C. T. Miller et al., pp. 115–125, Elsevier, New York.

Aris, R. (1956), On the dispersion of a solute in a fluid flowing through a tube, *Proc. R. Soc. London, Ser. A.*, 235, 67–77.

Bear, J. (1972), *Dynamics of Fluids in Porous Media*, 764 pp., Dover, Mineola, N. Y.

Blunt, M. J., M. D. Jackson, M. Piri, and P. H. Valvatne (2002), Detailed physics, predictive capabilities and macroscopic consequences for network models of multiphase flow, *Adv. Water Res.*, 25(8–12), 1069–1089.

Bolt, G. H. (1982), Movement of solutes in soil: Principles of adsorption/exchange chromatography, in *Soil Chemistry*, Part B, *Physico-chemical Models*, edited by G. H. Bolt, pp. 285–348, Elsevier, New York.

Bosma, W. J. P., and S. E. A. T. M. Van der Zee (1992), Analytical approximation for nonlinear adsorbing solute transport and first order degradation, *Transp. Porous Media*, 11, 33–43.

Bosma, W. J. P., and S. E. A. T. M. Van der Zee (1993), Transport of reactive solute in a one-dimensional, chemically heterogeneous porous medium, *Water Resour. Res.*, 29(1), 117–131.

Celia, M., P. C. Reeves, and L. A. Ferrand (1995), Recent advances in pore scale models for multiphase flow in porous media, *U.S. Natl. Rep. Int. Union Geod. Geophys. 1991–1994, Rev. Geophys.*, 33, 1049–1057.

Chandrasekhar, S. (1943), Stochastic problems in physics and astronomy, *Rev. Mod. Phys.*, 15, 1–89.

Chrysikopoulos, C. V., P. K. Kitanidis, and P. V. Roberts (1990), Analysis of one dimensional solute transport through porous media with spatially variable retardation factor, *Water Resour. Res.*, 26, 437–446.

De Josselin de Jong, G. (1958), Longitudinal and transverse diffusion in granular deposits, *Eos Trans. AGU*, 39, 6774.

Dullien, F. A. L. (1991), Characterization of porous media—Pore level, *Transp. Porous Media*, 6, 581–606.

Fatt, I. (1956), The network model of porous media, part I: Capillary characteristics, *Trans. Am. Inst. Min. Metall. Pet.*, 144–159.

Hassanizadeh, S. M., and W. G. Gray (1979), General conservation equations for multiphase systems, 1: Averaging procedures, *Adv. Water Res.*, 2, 131–144.

Hassanizadeh, S. M., M. A. Celia, and H. K. Dahle (2002), Dynamic effect in the capillary pressure-saturation relationship and their impacts on unsaturated flow, *Vadose Zone Hydrol.*, 1, 38–57.

Ioannidis, M. A., and J. Chatzis (1993), Network modelling of pore structure and transport properties of porous media, *Chem. Eng. Sci.*, 48(5), 951–972.

Keijzer, H., R. J. Schotting, and S. E. A. T. M. Van der Zee (2000), Semi-analytical traveling wave solution of one-dimensional aquifer bioremediation, *Commun. Appl. Nonlinear Anal.*, 7, 1–20.

Koplik, J. (1982), Creeping flow in two-dimensional networks, *J. Fluid. Mech.*, 119, 219–247.

Mohanty, K., and S. Salter (1982), Multiphase flow in porous media: II. Pore-level modeling, SPE paper 11018 presented at 57th Annual Fall Technical Conference and Exhibition of the Society of Petroleum Engineers of AIME, New Orleans, La.

Sahimi, M., A. Heiba, H. Davis, and L. Scriven (1986), Dispersion in flow through porous media—I. One phase flow, *Chem. Eng. Sci.*, 41(8), 2103–2122.

Serrano, S. E. (2003), Propagation of nonlinear reactive contaminants in porous media, *Water Resour. Res.*, 39(8), 1228, doi:10.1029/2002WR001922.

Sorbie, K. S., and P. J. Clifford (1991), The inclusion of molecular diffusion effects in the network modelling of hydrodynamic dispersion in porous media, *Chem. Eng. Sci.*, 46(10), 2525–2542.

Suchomel, B. J., B. M. Chen, and M. B. Allen (1998), Macroscale properties of porous media from a network model of biofilm processes, *Transp. Porous Media*, 31(1), 39–66.

Sugita, F., and R. W. Gillham (1995), Pore scale variation in retardation factor as a cause of nonideal reactive breakthrough curves, 3: Column investigations, *Water Resour. Res.*, 31(1), 121–128.

Sun, N.-Z. (1996), *Mathematical Modeling of Groundwater Pollution*, 377 pp., Springer, New York.

Taylor, G. (1953), Dispersion of solute matter in solvent flowing slowly through a tube, *Proc. R. Soc. London, Ser. A*, 219, 186–203.

Tsakiroglou, C. D., and A. C. Payatakes (2000), Characterization of the pore structure of reservoir rocks with the aid of serial sectioning analysis, mercury porosimetry and network simulation, *Adv. Water Res.*, *23*(7), 773–789.

Van Brakel, J. (1975), Pore space models for transport phenomena in porous media review and evaluation with special emphasis on capillary liquid transport, *Powder Technol.*, *11*, 205–236.

Van der Zee, S. E. A. T. M. (1990), Analytical traveling wave solutions for transport with nonlinear and nonequilibrium adsorption, *Water Resour. Res.*, *26*(10), 2563–2578. (Correction, *Water Resour. Res.*, *27*(5), 983.)

Van der Zee, S. E. A. T. M., R. C. Acharya, and G. M. C. M. Janssen (2004), Upscaling biogeochemically reactive chemical transport, in *Proceedings of International Workshop Saturated and Unsaturated Zone—Integration of Process Knowledge Into Effective Models, May 5–7, Rome, Italy*, edited by P. Aagaard et al., pp. 355–362, La Goliardica Pavese, Pavia, Italy.

Van Duijn, C. J., P. Knabner, and S. E. A. T. M. Van der Zee (1993), Traveling waves in the transport of reactive solutes through porous media: Combination of Freundlich and Langmuir isotherms, *Adv. Water Res.*, *16*, 97–105.

Van Genuchten, M. T., and W. J. Alves (1982), Analytical solutions of the one dimensional convective-dispersive solute transport equation, *USDA ARS Tech. Bull. 1661*, U.S. Salinity Lab., Riverside, Calif.

Verlaan, M. (2001), Dispersion in heterogeneous media: Fundamental issues inspired by underground gas storage, Ph.D. thesis, 145 pp., Delft Univ. of Technol., Delft, Netherlands.

Whitaker, S. (1969), Advances in the theory of fluid flow in porous media, *Ind. Eng. Chem.*, *12*, 14–28.

————————————————

R. C. Acharya and S. E. A. T. M. Van der Zee, Soil Quality Section, Department of Environmental Sciences, WUR, P.O. Box 47, 6700 AA Wageningen, Netherlands. (ram.acharya@wur.nl)

A. Leijnse, Department of Environmental Sciences, WUR, 6700 AA Wageningen, Netherlands.